Int. J. Heat Mass Transfer. Vol. 25, No. 8, pp. 1157–1166, 1982
Printed in Great Britain

0017-9310/82/081157-10 $03.00/0
Pergamon Press Ltd.

HOLOGRAPHIC INTERFEROMETRY MEASUREMENT OF CONVECTIVE HEAT TRANSPORT BENEATH A HEATED HORIZONTAL CIRCULAR PLATE IN AIR

R. E. FAW* and T. A. DULLFORCE
Culham Laboratory, UKAEA Research Group, Abingdon, Oxfordshire, U.K.

(*Received* 23 *January* 1981 *and in revised form* 25 *January* 1982)

Abstract—The technique of live-fringe holographic interferometry has been used in an investigation of convective heat transfer in air beneath a heated horizontal circular plate. Measurements were made beneath an 18.1 cm dia copper plate held at 16, 21 and 26 K above ambient temperature. This resulted in Rayleigh numbers of 1.07×10^6, 1.34×10^6 and 1.60×10^6. The paper describes apparatus and procedures used in the holographic process as well as methods used in deriving temperature profiles from interferograms. Measured temperature profiles and Nusselt numbers agreed with predictions based on approximate analytical solutions to the heat transfer problem previously reported by others.

NOMENCLATURE

a,	plate radius [m];
g,	acceleration of gravity [m s^{-2}];
K,	Gladstone–Dale constant [m^3 kg^{-1}];
n,	refractive index;
Nu,	Nusselt number;
p,	pressure [Pa];
R,	ideal gas constant [m^3 Pa kg^{-1} K^{-1}];
Ra,	Rayleigh number;
R, Y, Z,	spatial coordinates;
r, y, z,	R/a, Y/a, Z/a;
T,	temperature [K];
u,	$(1 - y^2)^{1/2}$;
v,	$(1 - r^2)^{1/2}$.

Greek symbols

α,	thermal diffusivity [m^2 s^{-1}];
β,	coefficient of thermal expansion [K^{-1}];
δ,	dimensionless boundary layer thickness [$2/Nu$];
ε,	fringe displacement;
η,	kinematic viscosity [m^2 s^{-1}];
θ,	$T - T_\infty$ [K];
λ,	wavelength [m];
ν,	$(a/\lambda)(n - n_\infty)$;
ρ,	density [kg m^{-3}];
ϕ,	$(T - T_\infty)/(T_0 - T_\infty)$.

Subscripts

0,	conditions at heat transfer plate ($z = 0$);
∞,	ambient conditions.

1. INTRODUCTION

MEASUREMENTS have been made of convective heat transport in air beneath the surface of an 18.1 cm dia horizontal circular plate, free at the edges and held at a constant temperature above that of the surroundings. The plate temperature was varied from 15 to 26 K above the ambient temperature. Live-fringe holographic interferometry was used to measure temperature profiles from which were determined convective heat transfer coefficients and boundary-layer thicknesses. Though many measurements have been made for rectangular plates, these are the first to be reported for a circular plate.

Figure 1 establishes the geometrical notation used here. Within the fluid, the dimensionless temperature index is

$$\phi(r, z) = \theta(r, z)/\theta_0 \tag{1}$$

where θ_0 is the plate temperature T_0 less the ambient temperature T_∞, and $\theta(r, z)$ is the local fluid temperature $T(r, z)$ less the ambient temperature. The Y direction is transverse to the direction of illumination and viewing of the plate. Dimensionless position indices are defined in terms of the characteristic plate dimension, viz. $r = R/a$. The Rayleigh and Nusselt numbers, defined in terms of the same characteristic length, are respectively

$$Ra = g\beta a^3\theta_0/\alpha\eta \tag{2}$$

and

$$Nu(r) = -\frac{\partial\phi}{\partial z}(r, 0). \tag{3}$$

The plate-average Nusselt number is

$$\overline{Nu} = 2\int_0^1 \mathrm{d}r\, r\, Nu(r). \tag{4}$$

A dimensionless index of the boundary layer thickness may be defined as

$$\delta(r) = 2/Nu(r). \tag{5}$$

*Present address: Nuclear Engineering Department, Kansas State University, Manhattan, Kansas, U.S.A.

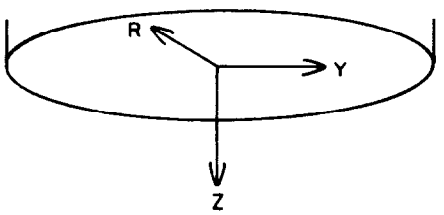

FIG. 1. Geometry for the downward heat transfer experiment. The plate surface temperature is T_0. Ambient temperature is T_∞. The laser beam is parallel to the plate surface and perpendicular to the y axis.

Experimental studies of downward heat transfer by convection from horizontal surfaces have built upon the early efforts of Weise [1], Saunders, Fishenden and Mansion [2], and Kraus [3], whose investigations established that, over a wide range of parameters, the Nusselt number for heat transfer was proportional to $Ra^{0.2}$ and only weakly dependent on the surface shape and edge conditions. Recent experimental studies include the work of Fujii and Imura [4] and Aihara, Yamada and Endo [5]. The former measured average Nusselt numbers for heat transfer to water from rectangular brass plates 5 cm × 10 cm × 0.5 cm thick and 15 cm × 30 cm × 1 cm thick. In an effort to establish 2-dim. flow patterns, the plate slides were insulated along the shorter dimensions. The uninsulated sides were presumably at or near the plate surface temperature. Over the range $10^6 \leq Ra \leq 10^{11}$ boundary layer flow was found to be laminar, with

$$\overline{Nu} = 0.58\, Ra^{0.2}. \tag{6}$$

Aihara and his co-workers studied heat transfer to air from a brass plate 25 cm × 35 cm × 1 cm thick. The shorter sides of the plate were insulated and the uninsulated sides were presumably at or near the plate surface temperature. Temperature profiles, measured using a thermocouple probe, and local Nusselt numbers were in substantial agreement with those predicted by Singh and Birkebak [6] for an infinite strip.

Birkebak and Abdulkadir [7] investigated heat transfer to water from a 19 cm square aluminum plate 1.25 cm thick. By a special cooling system, the plate sides were held at ambient temperature. Except near the edges of the plate, temperature profiles, measured using a thermocouple probe, and local Nusselt numbers were in agreement with predictions of Singh, Birkebak and Drake [8] for a square plate. In agreement with previous observations, [1–5] the boundary-layer thicknesses were found to be finite at the plate edges. The average Nusselt number over the entire plate surface was found to be

$$\overline{Nu} = 0.68\, Ra^{0.2}. \tag{7}$$

Restrepo and Glicksman [9] studied heat transfer to air from a copper plate 7 in. × 7 in. × 1 in. thick with side surfaces insulated, heated to the plate surface temperature, or cooled to ambient temperature. Temperature profiles were measured using a thermocouple probe. At the plate edges, boundary-layer thicknesses were much greater for the cooled sides than for the heated sides and for the former were as thick as 1/8 the plate dimensions. For plates with heated sides, plate-average Nusselt numbers agreed with equation (6).

Analytical studies of downward convection from plates have been carried out using the boundary-layer approximation. Stewartson [10] and Gill, Zeh and del Casal [11] obtained similarity solutions for a 2-dim. case. Integral methods were applied by Levy [12] and Wagner [13] for the semi-infinite strip. The method was extended [8] to rectangular and circular plates. These analyses involved assuming the thermal boundary layer to vanish at the plate edge. For the special case of the infinite strip [6] solutions have been obtained accommodating finite boundary-layer thicknesses at the plate edge [6].

For the circular plate, the subject of this experimental study, the analysis in ref. [8] leads to temperature profiles of the form

$$\phi(r, z) = \left[1 - \frac{z}{\delta(r)}\right]^2 \tag{8}$$

in which, to a first-order approximation,

$$\delta(r) = \delta_0 v^{1/2}(r) \tag{9}$$

with

$$\delta_0 = \delta(0) = 4.104\, Ra^{-1/5} \tag{10}$$

and

$$v(r) = (1 - r^2)^{1/2}. \tag{11}$$

The local Nusselt number is thus

$$Nu(r) = 2/\delta(r) = 0.487\, v^{-1/2}(r)\, Ra^{1/5}. \tag{12}$$

2. EXPERIMENTAL PROCEDURE

Measurements were made of temperature profiles in air beneath the surface of a heated, downward-facing, horizontal plate using live-fringe holographic interferometry. A general discussion of the techniques and apparatus has been presented elsewhere [14]. Using an argon-ion laser, a hologram was made of the plate and its surroundings, all at ambient temperature. The plate temperature was then increased, while the hologram and plate were illuminated by the laser light under conditions otherwise identical to those during the preparation of the hologram. The hologram image was superimposed on the real plate and surroundings. Changes in refractive index of the heated air led to optical interference patterns which were recorded photographically. From the interference patterns were

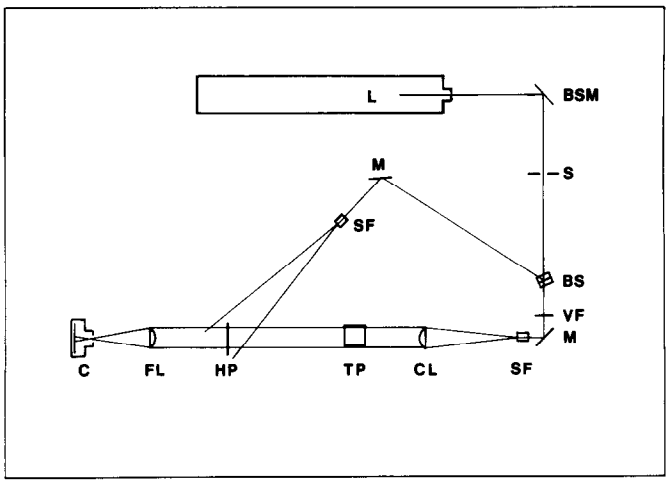

FIG. 2. Experimental arrangement for holographic interferometry. L, laser; BP, beam positioning mirrors; S, shutter; BS, beam splitter; M, mirror; VF, variable filter; SF, spatial filter; CL, collimating lens; TP, heat transfer test plate; HP, hologram plate; FL, focusing lens and C, camera.

determined temperature profiles and Nusselt numbers using procedures described below.

The overall arrangement of apparatus is illustrated in Fig. 2. Apparatus was positioned on a granite bench, 4 ft × 10 ft × 4 in. thick. Isolation from vibration was provided by supporting the bench at each corner on lightly inflated rubber-tyre tubes. The tubes rested on sand-filled concrete cylinders. The cylinders rested on a sand base in larger concentric concrete cylinders, also sand-filled. (For further details, see ref. [14]).

The beam from an argon-ion laser was elevated to 26 cm above the bench by a pair of beam-positioning mirrors. After passing through a shutter, the beam was divided into two equal components by a beam-splitting cube. One beam, the reference beam, was expanded by a × 20 microscope objective and filtered by an 11 μm dia. pin hole. The objective was located 85 cm from the hologram plate and the expanded beam struck the plate at an angle of about 45°. A second beam, the object beam, was expanded and filtered by a 20 × objective and 11 μm pin hole and collimated by a 15 cm dia., 20 cm focal length lens located 38 cm from the center of the heat transfer plate. A variable density filter was used to adjust the intensity of the object beam. The X-axis of the heat transfer plate (Fig. 1) was aligned with the axis of the object beam.

The laser used was a high-power, argon-ion laser, Spectra-Physics Model 171-06. It had a nominal power rating of 9 W (multi-line) and 3.75 W (514.5 nm line). Available power was considerably in excess of rated power. Single-frequency operation was made possible by the use of an etalon, Spectra-Physics Model 589, in the laser cavity. With the etalon in use, available power at 514.5 nm was about 2.5 W. Laser beam diameter (e^{-2} points) was nominally 1.6 mm with a full-angle beam divergence of 0.72 mrad.

Mirrors, beam expanders, positioners, splitters and spatial filters were components distributed by Ealing–Beck Ltd. For high-power operation, uncemented microscope objectives, manufactured by W. R. Prior, were used. The reference-beam mirror was a 4 in. dia Schlieren-quality mirror made by Optical works Ltd. The hologram plate holder was a Micro-Controle, Type SH37 Plate Support distributed by Unimatic Engineers Ltd. Hologram plates were 8E56 (AHI) Holotest Plates made on speical order by Agfa-Gevaert Ltd. The plates were 4 in. × 5 in. with thickness 1.5–1.7 mm. Plate flatness is 25 μm/in or better.

The heat transfer plate was a circular copper plate, 18.1 cm dia and 1.21 cm thick, free at the edges, shown in silhouette in Figs. 3–5. Thermocouple wells, 1.6 mm dia, were drilled to 1 mm from the plate surface. Wells were located at radii of 0, 2.54, 5.08, 6.99 and 8.81 cm. The plate was heated by four circular nichrome heating elements cemented into grooves in an insulating backing plate (0.572 cm thick asbestos board). The heating elements were connected in series and were spaced to provide approximately uniform heating (3.8, 6.4, 7.6 and 8.4 cm radii). The elements were powered through variable transformers connected to 240 V, 50 Hz mains power. To facilitate adjustment, a variable resistor (22 Ω, 10 A rating) was placed in series with the heating elements. With these arrangements, the plate temperature was easily held uniform to within 0.5 K. The insulating plate was backed by a 0.85 cm thick perspex plate from which supporting connections were made.

The test plate was levelled and aligned using the horizontal unexpanded object beam from the laser. The laser beam was also used to align the camera used to photograph interference patterns. With the alignment beam along the centre-line of the plate, the levelled camera was positioned so that the beam passed through the aperture at its smallest stop and through the centre of the film-holder. To minimize effects of air currents, the test plate was surrounded on

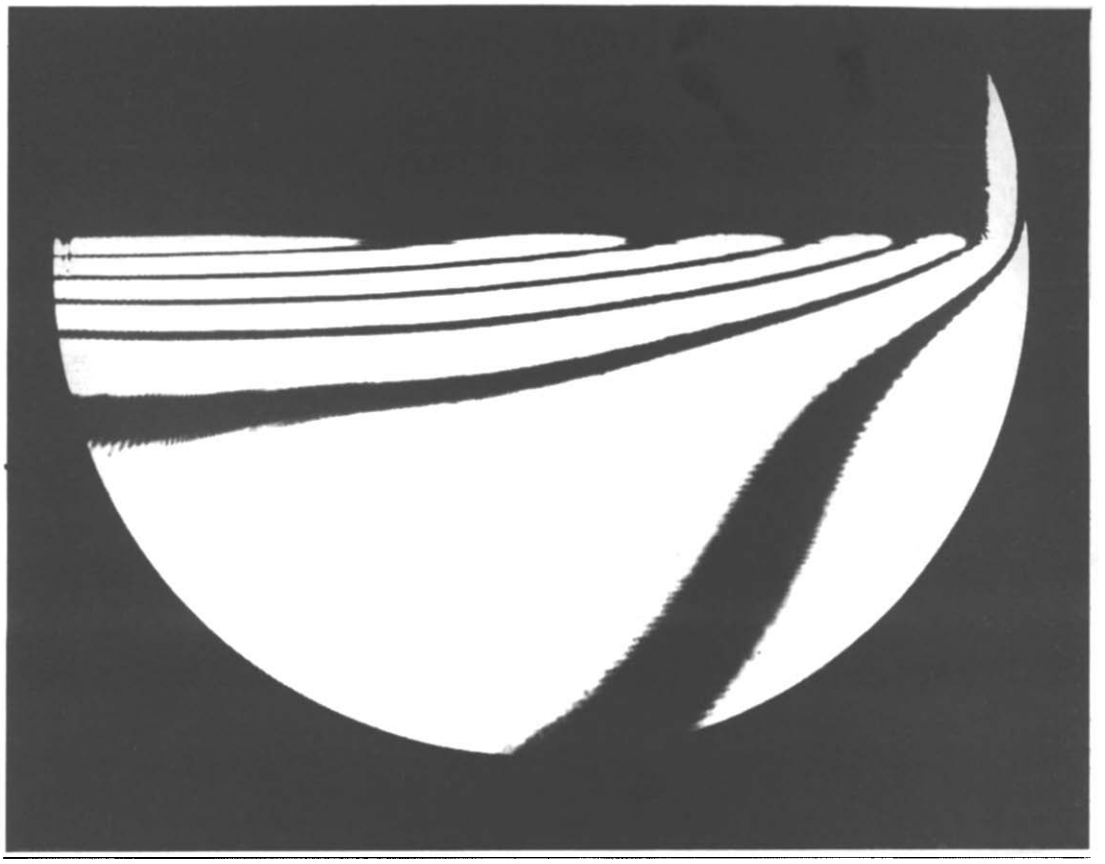

FIG. 3. Infinite fringe interferogram for $\theta_0 \simeq 18\,\mathrm{K}$.

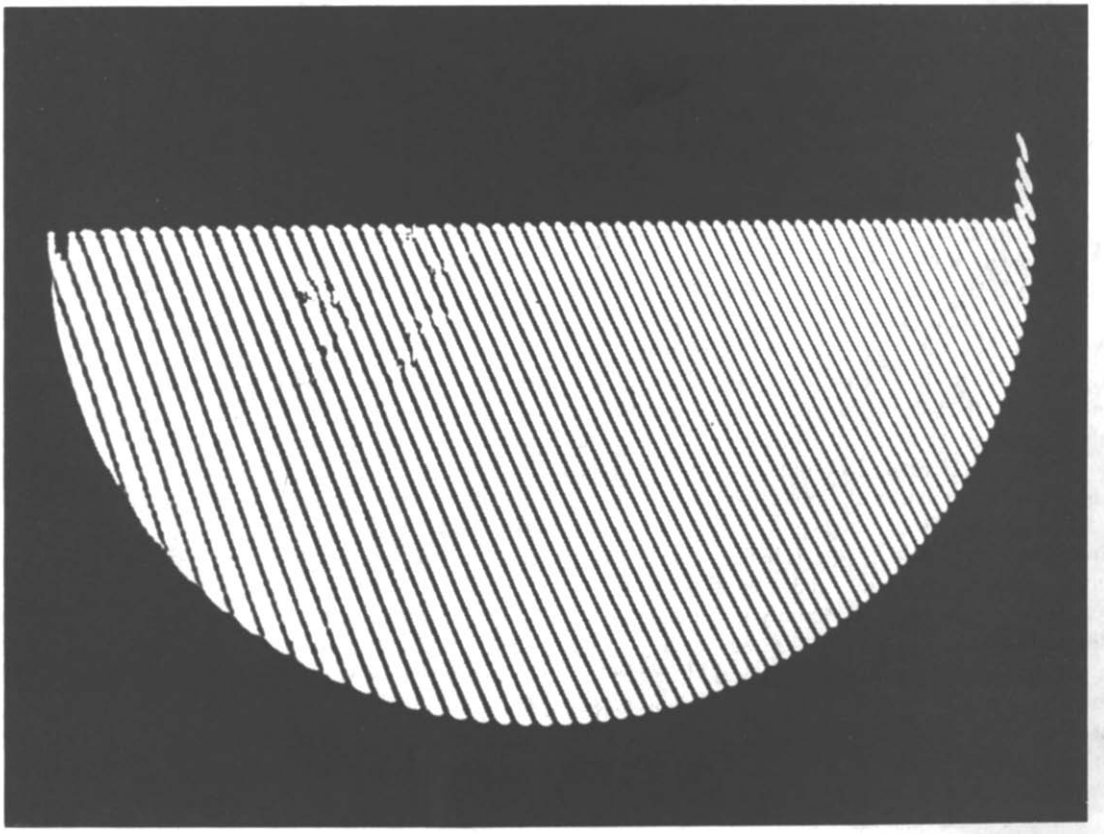

FIG. 4. Finite fringe interferogram for $\theta_0 = 0\,\mathrm{K}$.

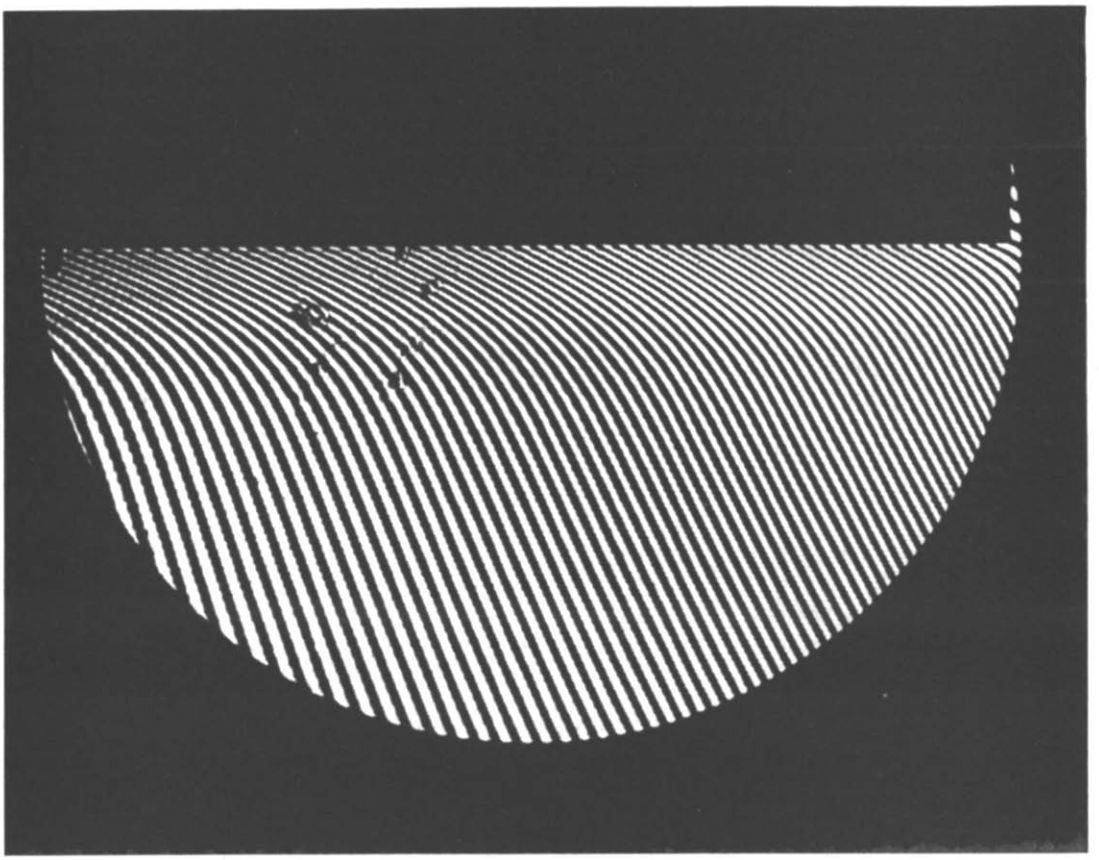

FIG. 5. Finite fringe interferogram for $\theta_0 = 26\,\text{K}$.

four sides by a glass-windowed enclosure made of heavy cardboard. The enclosure was open at the top and had air entrance slits at its base.

With the heat transfer plate at ambient temperature, a hologram plate was exposed to an incident energy density of about $5\,\mu\text{J}\,\text{cm}^{-2}$, with the intensity of the reference beam twice that of the object beam. The hologram plate was processed using a procedure similar to that described by Phillips and Porter [15]. The essential features were developed in undiluted Neofin Blau (Tetenal Photowerk), and bleaching in an aqueous solution of ferric nitrate, potassium bromide and isopropanol.

With the heat transfer test plate still at ambient temperature, the hologram plate was carefully re-positioned in its holder and illuminated by the object and reference beams. A virtual holographic image of the test plate was then displaced slightly to produce a system parallel interference fringes (Fig. 4), the so-called finite-fringe setting. Power was then applied to the heating elements of the test plate. The plate temperature was increased at a rate of about $1\,\text{K}\,\text{min}^{-1}$ and at the same time carefully monitored to assure uniformity. Convective heat transfer from the plate caused density changes and corresponding refractive index changes in the air. These changes caused optical interference leading to distortion of the fringes.

Interference patterns were photographed on microfilm (Eastman Kodak 5669 Micro-File) using a 35 mm SLR camera (Asahi Pentax KX) with a 50 mm focal length $f/1.7$ lens, augmented by a 15 cm dia, 60 cm focal length lens (Tropel 280–150). Typical exposure time was 1/250 s with the laser power at 50 mW. The microfilm was processed using Teknol developer (May & Baker Ltd.).

3. DATA ANALYSIS

Raw experimental data were in the form of photographic records of interference patterns. Figure 3 is an interferogram for $\theta_0 \simeq 18\,\text{K}$. This corresponds to the infinite-fringe setting of the Mach–Zehnder interferometer and was produced by double-exposure holographic interferometry. This infinite-fringe setting was difficult to achieve experimentally, and an alternate approach was used, the finite-fringe setting.

Figure 4 exhibits deliberately introduced finite fringes, with $T_0 = T_\infty = 294\,\text{K}$, i.e. $\theta_0 = 0\,\text{K}$. The hologram plate was exposed under the prescribed conditions, but rotated very slightly about its vertical axis when re-positioned in its holder. Figure 5 exhibits the interferogram after the plate temperature had been brought to 319 K ($\theta_0 = 26\,\text{K}$). Adjacent pairs of light or dark fringes result from a change of one wavelength (514.5 nm) in the optical path length of the object beam between the conditions when the hologram was made

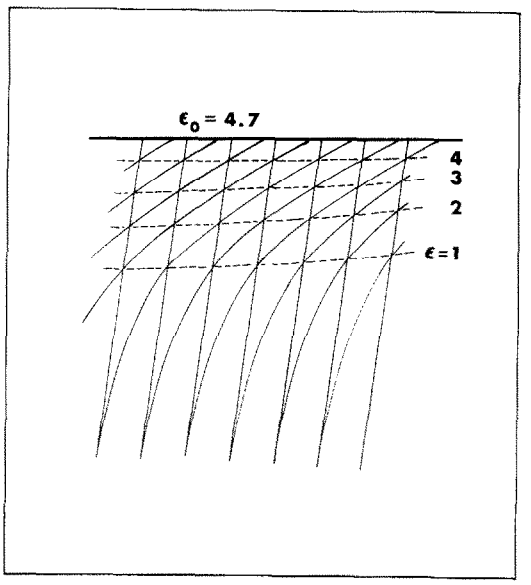

FIG. 6. Superposition of interferograms to determine fringe displacement.

and the conditions under observation. Differences between the interferograms of Figs. 4 and 5 are due to density changes in the air beneath the plate. Superposition of Figs. 4 and 5, shown schematically in Fig. 6, allows measurement of fringe displacement $\varepsilon(y, z)$ as a function of position. Figure 7 shows the loci of fringe displacements for Figs. 4 and 5. The procedure for determining fringe displacement was as follows. Prints of the microfilm records were made on Eastman Kodak 4556 Reproduction Film at an enlargement of about three times actual size. Films for Figs. 4 and 5, for example, were superimposed over an illuminated background and values of $\varepsilon(y, z)$ were scaled directly from the films.

Temperature profiles were determined from fringe displacements in the following manner. Since unit fringe displacement results from a change of one wavelength in optical path, the measured displacement is related to the variation in refractive index $n(r, z)$ of the air by the equation [16]

$$\varepsilon(y, z) = 2 \int_y^1 \frac{\mathrm{d}r\, r\, v(r, z)}{(r^2 - y^2)^{1/2}} \tag{13}$$

where

$$v(r, z) = (a/\lambda)\,[n_\infty - n(r, z)] \tag{14}$$

and n_∞ is the refractive index at ambient temperature. The function $v(r, z)$ may be determined from measured values of $\varepsilon(y, z)$ by the inversion [16]

$$v(r, z) = -\pi^{-1} \int_r^1 \frac{\mathrm{d}y}{(y^2 - r^2)^{1/2}} \frac{\partial \varepsilon}{\partial y}(y, z). \tag{15}$$

An alternative, and computationally more efficient, inversion may be accomplished in terms of the variables u and v. Then

$$\varepsilon(u, z) = 2 \int_0^u \frac{\mathrm{d}v\, v\, v(v, z)}{(u^2 - v^2)^{1/2}} \tag{16}$$

and

$$v(v, z) = \pi^{-1} \int_0^v \frac{\mathrm{d}u}{(v^2 - u^2)^{1/2}} \frac{\partial \varepsilon}{\partial u}(u, z). \tag{17}$$

According to the Gladstone–Dale law, the variation with density ρ of the refractive index of a gas is closely approximated by

$$\frac{\mathrm{d}n}{\mathrm{d}T} = K \frac{\mathrm{d}\rho}{\mathrm{d}T} \tag{18}$$

were K is the Gladstone–Dale constant (0.2226 $\mathrm{cm^3 g}$

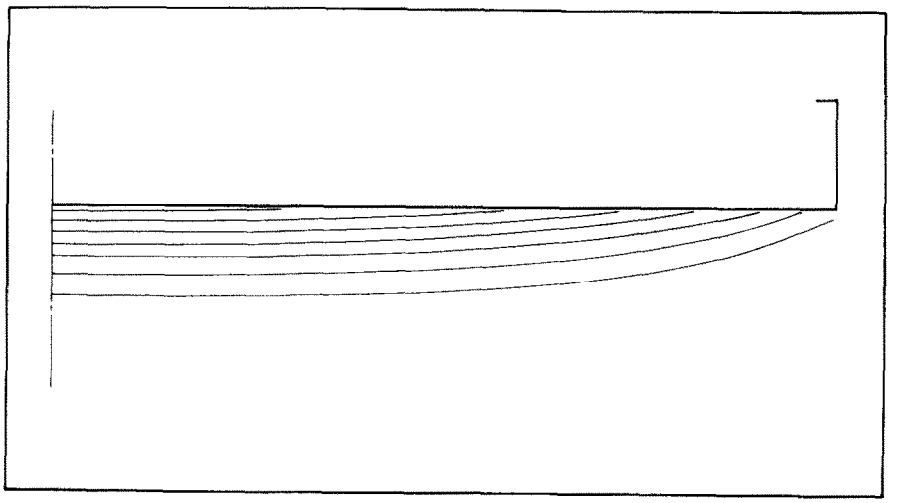

FIG. 7. Loci of fringe displacements for $\theta_0 = 26\mathrm{K}$.

for air). Assuming ideal gas behaviour, $d\rho/dT = -p/RT^2$, thus

$$\frac{dn}{dT} = -\frac{Kp}{RT^2} \tag{19}$$

where p is the ambient pressure and R the ideal gas constant. Thus, upon integration of equation (19) and application of equation (14)

$$v = C(T_\infty^{-1} - T^{-1}) \tag{20}$$

where $C = Kpa/R\lambda = 13760 \pm 70\,\text{K}$. Since $\theta_0 = T_0 - T_\infty$, it follows from equation (20) that

$$\theta = vTT_\infty/C \tag{21}$$

and

$$\phi = \theta/\theta_0 = vT/v_0T_0 \simeq v/v_0 \tag{22}$$

The approximation $T/T_0 \simeq 1$ in equation (22) is valid to within a few percent for the measurements reported in this paper. On the basis of this approximation

$$Nu(v) = -\frac{1}{v_0}\frac{\partial v}{\partial z}(v, 0). \tag{23}$$

Equation (22), combined with equation (8) leads to the following as an approximation based on theory:

$$v(v, z) \simeq v_0(1 - z/\delta_0 v^{1/2})^2 \tag{24}$$

Substitution of equation (24) into equation (16) yields the following approximation for $\varepsilon(u, z)$:

$$\varepsilon/2v_0u \simeq (1 - \sigma^4)^{1/2} + \sigma^2\cos^{-1}\sigma^2 + 2^{3/2}\sigma F \times (\cos^{-1}\sigma, 2^{-1/2}) - 2^{5/2}\sigma E(\cos^{-1}\sigma, 2^{-1/2}) \tag{25}$$

where

$$\sigma = z/\delta_0 u^{1/2} \tag{26}$$

and F and E are, respectively, elliptic integrals of the first and second kind.

4. RESULTS AND DISCUSSION

Raw experimental data are presented in Table 1. For each plate temperature and each y position, measurements were made of z positions for integral fringe displacements. Random measurement error in z is about $\pm$ 0.0005. Systematic error in z due to imprecise location of the plate surface ($z = 0$) is also about $\pm$ 0.0005. Uncertainty in T_∞ is 0.5 K.

Equation (25) indicates that, based on the approximate theory, for given θ_0, ε/u is a function of $z/u^{1/2}$. Experimentally this was found to be true, as exhibited in Fig. 8. Indeed, data were well fit by the approximation

$$(\varepsilon/u)^{1/2} = C_1 - C_2 z/u^{1/2}. \tag{27}$$

Least-squares regression analyses yielded values of C_1 and C_2 listed in Table 2. The uncertainties cited combine the estimated standard deviations from the regression analyses and the effects of the possible systematic error in the z position. Uncertainties for the other parameters listed in the table were propagated by standard statistical methods.

Substitution of equation (27) into equations (17), (23) and (5) yields

$$v_0 = C_1^2/2, \tag{28}$$

$$Nu(v) = \frac{1.66925\ C_2}{C_1 v^{1/2}} \tag{29}$$

and

$$\delta_0 = \frac{1.19814\ C_1}{C_2}. \tag{30}$$

Values for T_0 and θ_0 were determined from equations (20) and (21) using the values of v_0 from equation (28).

Experimental results, expressed as $(\varepsilon/2uv_0)^{1/2}$ vs $z/\delta_0 u^{1/2}$ are illustrated in Fig. 8 and compared with the theoretical prediction given by equation (25). Temperature profiles are described by $\phi \simeq v/v_0$. The experimental profiles may be determined by substitution of equation (27) into equation (17), with the result

$$\frac{v(v, z)}{v_0} = \frac{2}{\pi}[\cos^{-1}s^2 - 2^{1/2}sF(\cos^{-1}\sigma, 2^{-1/2})] \tag{31}$$

where

$$s = \frac{C_2 z}{C_1 v^{1/2}} = \frac{1.19814\, z}{\delta_0 v^{1/2}}. \tag{32}$$

Note that the inversion integration of equation (17) was carried out analytically using equation (27) for $\varepsilon(u, z)$ rather than numerically using raw experimental data. This experimental result is compared with the approximate theoretical result, equation (24), in Fig. 9.

Figures 8 and 9 demonstrate excellent agreement between measured temperature profiles and those predicted in ref. [8]. Equation (8) is apparently a very good representation of the temperature profile beneath a heated circular plate. Likewise the radial dependence of the boundary layer thickness δ apparently is represented well by equation (9). It must be pointed out, though, that in equation (8) the distance z from the plate surface is normalized by the boundary

Table 1. Raw experimental data: values of z for mixed ε and y at three values of θ_0

ε	θ_0 (K)	y 0	0.1	0.2	0.3	0.4	0.5	0.6	0.7	0.8	0.9	0.95
1	26	0.115	0.115	0.115	0.114	0.111	0.107	0.103	0.0936	0.0793	0.0551	0.0380
	21	0.120	0.120	0.118	0.117	0.116	0.114	0.109	0.0999	0.0819	0.0542	0.0382
	16	0.122	0.120	0.118	0.114	0.109	0.100	0.090	0.0779	0.0614	0.0389	0.0244
2	26	0.0817	0.0817	0.0817	0.0813	0.0798	0.0767	0.0716	0.0620	0.0490	0.0267	0.0118
	21	0.0819	0.0803	0.0789	0.0772	0.0758	0.0723	0.0661	0.0573	0.0435	0.0225	0.0088
	16	0.0767	0.0750	0.0729	0.0697	0.0654	0.0591	0.0510	0.0409	0.0261		
3	26	0.0639	0.0639	0.0639	0.0639	0.0606	0.0563	0.0502	0.0406	0.0270	0.0072	
	21	0.0575	0.0564	0.0545	0.0527	0.0506	0.0469	0.0415	0.0321	0.0186		
	16	0.0474	0.0462	0.0443	0.0413	0.0368	0.0313	0.0236	0.0121			
4	26	0.0481	0.0481	0.0469	0.0447	0.0423	0.0380	0.0313	0.0217	0.0084		
	21	0.0368	0.0349	0.0340	0.0328	0.0316	0.0263	0.0200	0.0105			
	16	0.0207	0.0197	0.0188	0.0161	0.0118	0.0072					
5	26	0.0337	0.0337	0.0315	0.0296	0.0261	0.0214	0.0154	0.0077			
	21	0.0201	0.0184	0.0167	0.0152	0.0128	0.0072					
6	26	0.0190	0.0192	0.0171	0.0159	0.0126	0.0067					
7	26	0.0084	0.0067									

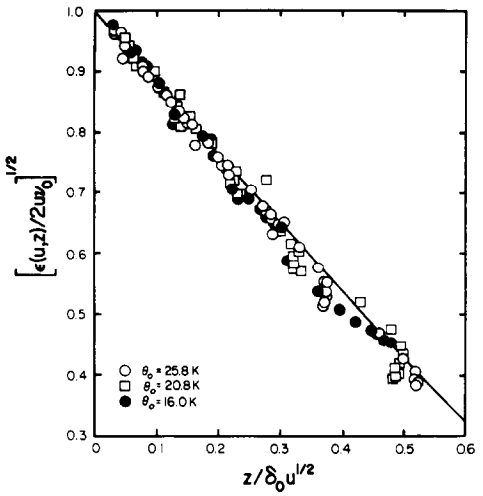

FIG. 8. Experimental data shown in comparison with approximate theoretical predictions, as depicted by the solid line [equation (25)].

Table 2. Summary of experimental results

θ_0	16.0 ± 0.2	20.8 ± 0.3	25.8 ± 0.3
C_1	2.200 ± 0.015	2.485 ± 0.022	2.748 ± 0.016
C_2	10.33 ± 0.18	12.10 ± 0.28	14.83 ± 0.16
v_0	2.419 ± 0.033	3.088 ± 0.048	3.777 ± 0.044
T_0	310.0 ± 0.6	314.8 ± 0.6	319.8 ± 0.7
$v^{1/2}Nu$	7.84 ± 0.14	8.13 ± 0.20	9.01 ± 0.11
δ_0	0.255 ± 0.005	0.246 ± 0.006	0.222 ± 0.003

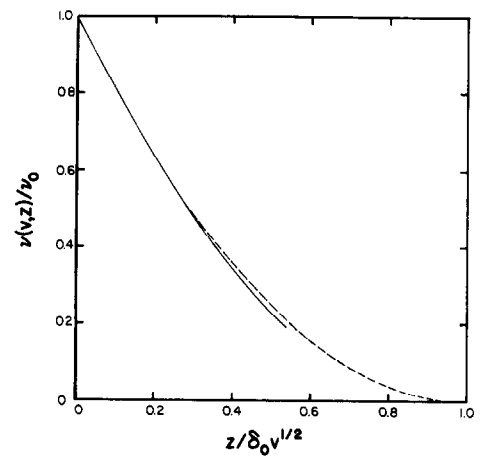

FIG. 9. Experimentally determined [equation (31), solid line] and theoretically predicted [equation (24), broken line] temperature profiles as described by $v(v, z)$.

Table 3. Comparison between measured and predicted Nusselt numbers at plate centre

	θ_0 16.0	20.8	25.8
Ra	1.07×10^6	1.34×10^6	1.60×10^6
Nu_{exp}	7.84 ± 0.14	8.13 ± 0.20	9.01 ± 0.11
Nu_{th}	7.83	8.18	8.47

layer thickness. However, our measured values of the boundary layer thicknesses, or equivalently the Nusselt numbers, are also in good agreement with predicted values of equations (10) and (12). A comparison between measured and predicted Nusselt numbers is given in Table 3. In the table, the Rayleigh numbers are evaluated at the mean between T_∞ and T_0. Within that range of temperature the Rayleigh number varies by about $\pm$ 20% but, since the Nusselt number is expected to vary with $Ra^{0.2}$ number, this variation in Rayleigh numbers would not account for the differences between measured and predicted Nusselt numbers. That measured Nusselt numbers exceed predicted values is expected, since the analysis leading to equation (12) is based on the assumption that the boundary layer vanishes at the plate edge. A finite boundary layer at the plate edge was observed in this study and by others [1–3, 5] in previous investigations.

Acknowledgements—The continued support of the UKAEA Safety and Reliability Directorate, Culcheth is gratefully acknowledged. We would also like to thank N. Boucher and R. Davies for their help in constructing apparatus.

REFERENCES

1. R. Weise, Wärmeübergang durch freie Konvection an quadratischen Platten, *Forsch Geb. Ing. Wes.* **6**, 281–292 (1935).
2. O. A. Saunders, M. Fishenden and H. D. Mansion, Some measurements of convection by an optical method, *Engineering, Lond.* 483–485 (1935).
3. W. Kraus, Temperatur- und Geschwindigkeitsfeld bei freier Konvektion um eine waagerechte quadratische Platte, *Physik. Z.* **4**, 126–150 (1940).
4. T. Fujii and H. Imura, Natural convection heat transfer from a plate with arbitrary inclination, *Int. J. Heat Mass Transfer* **15**, 755–767 (1972).
5. T. Aihara, Y. Yamada and S. Endo, Free convection along the downward-facing surface of a heated horizontal plate, *Int. J. Heat Mass Transfer* **15**, 2535–2549 (1972).
6. S. N. Singh and R. C. Birkebak, Laminar free convection from a horizontal infinite strip facing downwards, *Z. Angew. Math. Phys.* **20**, 454–461 (1969).
7. R. C. Birkebak and A. Abdulkadir, Heat transfer by natural convection from the lower side of finite horizontal heated surface, Vol. 4, Paper NC2.2, *Heat Transfer Conf.*, Paris (1970).
8. S. N. Singh, R. C. Birkebak and R. M. Drake Jr., Laminar free convection heat transfer from downward-facing horizontal surfaces of finite dimensions in *Progress in Heat and Mass Transfer*, Vol. II, pp. 87–98. Pergamon Press, Oxford (1969).
9. F. Restrepo and L. R. Glicksman, The effect of edge conditions on natural convection from a horizontal plate, *Int. J. Heat Mass Transfer* **17**, 135–142 (1974).

10. K. Stewartson, On the free convection from a horizontal plate, *Z. Angew. Math. Phys.* **9a**, 276–282 (1958).
11. W. N. Gill, D. W. Zeh and E. del Casal, Free convection on a horizontal plate, *Z. Angrew. Math. Phys.* **16**, 539–541 (1965).
12. S. Levy, Integral methods in natural-convection flow, *J. Appl. Mech.* **22**, 515–522 (1955).
13. C. Wagner, Discussion on integral methods in natural convection flow, *J. Appl. Mech.* **23**, 320–321 (1956).
14. R. E. Faw and T. A. Dullforce, Holographic interferometry principles and procedures, Report CLM-RR/S2/19, Culham Laboratory, UKAEA Research Group, Abingdon, Oxfordshire (1977).
15. N. J. Phillips and D. Porter, An advance in the processing of holograms, *J. Phys. E., Sci. Inst.* **9**, 631–634 (1976).
16. R. J. Goldstein, Optical techniques for temperature measurement, in *Measurements in Heat Transfer*, (edited by E. R. G. Eckert and R. J. Goldstein) Ch. 5. McGraw-Hill, New York (1976).

MESURE PAR INTERFEROMETRIE HOLOGRAPHIQUE DE LA CONVECTION THERMIQUE AUTOUR D'UNE PLAQUE CIRCULAIRE HORIZONTALE CHAUFFEE DANS L'AIR

Résumé—La technique de l'interférométrie holographique a été utilisée dans une étude du transfert convectif de chaleur dans l'air autour d'une plaque circulaire horizontale et chauffée. Des mesures sont effectuées près d'une plaque de cuivre de 18,1 cm de diamètre, maintenue à 16, 21 et 26 K au dessus de la température ambiante. Ceci conduit à des nombres de Rayleigh de $1{,}07 \times 10^6$, $1{,}34 \times 10^6$ et $1{,}60 \times 10^6$. On décrit l'appareillage et le mode opératoire suivi dans le processus holographique aussi bien que les méthodes utilisées pour obtenir les profils de température à partir des interférogrammes. Les profils de température mesurés et les nombres de Nusselt s'accordent avec les précisions basées sur des solutions analytiques approchées du problème de transfert thermique antérieurement traités par d'autres.

MESSUNG DES KONVEKTIVEN WÄRMEÜBERGANGS IN LUFT UNTERHALB EINER HORIZONTALEN, KREISRUNDEN, BEHEIZTEN PLATTE MIT HILFE DER HOLOGRAFISCHEN INTERFEROMETRIE

Zusammenfassung—Mit dem Verfahren der kontinuierlichen holografischen Interferometrie wurde der konvektive Wärmeübergang in Luft unterhalb einer beheizten, horizontalen, kreisrunden Platte untersucht. Die Messungen wurden an einer Kupferplatte mit 18,1 cm Durchmesser durchgeführt, die 16; 21 und 26 K über Umgebungstemperatur gehalten wurde. Dies hatte Rayleigh-Zahlen von $1{,}07 \times 10^6$; $1{,}34 \times 10^6$ und $1{,}60 \times 10^6$ zur Folge. Die Arbeit beschreibt sowohl die Apparatur und Arbeitsweise des holografischen Verfahrens als auch die Methoden zur Ermittlung der Temperaturprofile aus den Interferogrammen. Die gemessenen Temperaturprofile und Nusselt-Zahlen stimmten gut mit Berechnungen überein, die auf einer analytischen Näherungslösung des Wärmeübergangsproblems basieren und von anderen Autoren veröffentlicht wurden.

ИЗМЕРЕНИЕ КОНВЕКТИВНОГО ТЕПЛОПЕРЕНОСА В ВОЗДУХЕ ПОД НАГРЕВАЕМОЙ ГОРИЗОНТАЛЬНОЙ КРУГЛОЙ ПЛАСТИНОЙ С ПОМОЩЬЮ МЕТОДА ГОЛОГРАФИЧЕСКОЙ ИНТЕРФЕРОМЕТРИИ

Аннотация — Голографическим интерференционным методом «живых полос» исследован конвективный теплоперенос в воздухе под нагреваемой горизонтальной круглой пластиной. В экспериментах использовалась медная пластина диаметром 18,1 см, нагреваемая до температуры на 16, 21 и 26 К выше окружающей. В этих случаях число Релея достигало значений, равных $1{,}07 \times 10^6$, $1{,}34 \times 10^6$ и $1{,}60 \times 10^6$. Дано описание прибора и техники голографических измерений, а также методов получения профилей температуры из интерферограмм. Температурые профили и значения числа Нуссельта согласуются с результатами приближенных аналитических решений задачи теплопереноса, полученными ранее другими авторами.